

# Numerical Analysis of Flow Channel Expansion and Contraction Effects on Polymer Electrolyte Membrane Fuel Cell Performance

E. Zardini, F. Bagherighajari, J.C. Pascoa, M. Abdollahzadehsangroudi

Departamento de Engenharia Eletromecânica, C-MAST – Center for Mechanical and Aerospace Sciences and Technologies, Universidade da Beira Interior  
Calçada Fonte do Lameiro, 6201-001 Covilhã, Portugal

[e.zardini@studenti.unibs.it](mailto:e.zardini@studenti.unibs.it); [f.bagherighajari@ubi.pt](mailto:f.bagherighajari@ubi.pt); [pascoa@ubi.pt](mailto:pascoa@ubi.pt); [mm.abdollahzadeh@ubi.pt](mailto:mm.abdollahzadeh@ubi.pt)

**Abstract** - This study numerically investigates the impact of flow channel expansion and contraction, specifically in "converging-diverging" and "tapered" configurations, on the performance of proton exchange membrane (PEM) fuel cells. A three-dimensional, multi-component, multiphase, and non-isothermal model was employed to simulate the PEM fuel cell performance under these configurations. Key performance metrics, including polarization curves, cathode reactant distribution, liquid water accumulation, and transverse flow patterns, were analyzed for various expansion/contraction flow channel designs and compared with parallel flow field configurations under reference conditions. The results demonstrate that expansion/contraction flow channels enhance reactant transport to the catalyst layer, increase reaction rates, and improve liquid water removal efficiency. At reference conditions, the converging-diverging configuration exhibited the highest performance, increasing net power density by 10% compared to the parallel flow field. This improvement underscores its effectiveness in facilitating reactant transport and liquid water expulsion, leading to superior overall performance.

**Keywords:** Numerical simulation, Flow field effect, enhanced mass transport, water management

## 1. Introduction

The need for clean energy production is critical for reducing greenhouse gas emissions, as over 80% of global carbon dioxide (CO<sub>2</sub>) emissions stem from natural energy and resource consumption [1]. Polymer electrolyte membrane fuel cells (PEMFCs) offer a promising solution due to their carbon-free operation. Unlike batteries that store energy, fuel cells are electrochemical devices that continuously convert the chemical energy of fuel into direct current (DC) electricity as long as reactant gases (fuel and air) are supplied.

Several factors influence PEMFC performance, including operating conditions, geometric parameters, flow field design, collector configuration, and membrane characteristics. Enhancing performance is essential to making PEMFCs a cost-effective alternative to conventional energy sources. Various strategies have been explored to improve their efficiency and operational stability. Zhang and Shi [2] evaluated the impact of channel dimensions on serpentine flow fields, finding that an eight-channel complex flow field achieved superior performance. Abdulla and Patnaikuni [3] demonstrated the advantages of using an Enhanced Cross Flow Split Serpentine Flow Field (ECSSFF) as the cathode channel, paired with a parallel anode design. Choi et al. [4] studied the effect of varying channel heights and widths, revealing that taller channels reduce pressure drop but may lead to water accumulation, slightly lowering performance. Zhang et al. [5] analyzed a converging-diverging flow field pattern, showing it outperforms conventional straight channels in efficiency.

Among various PEMFC flow field designs, tapered and converging-diverging flow channels can provide uniform reactant distribution and water removal under reasonable pressure drop. Xu et al. [6] investigated how the aspect ratio and sidewall angle affect flow distribution in a tapered channel-shaped FFC. Their findings showed that these factors significantly influence flow distribution within the channel. Wang et al. [7] then constructed two tapered flow fields for fuel cells with different channel heights and widths and conducted experiments and simulations. The results show that the steeper the channel slope, the smaller the depth and width, and the better the fuel cell performance.

While prior research has extensively examined conventional flow channel designs (e.g., straight, serpentine, interdigitated) and their dimensions (e.g., length, height, width, and cross-sectional shapes), this study focuses on comparing conventional, tapered, and converging-diverging configurations, including modified versions such as half-tapered and half-

converging-diverging channels. Additionally, the effects of flow direction—whether fuel is introduced at the inlet or outlet of the channels—are evaluated. This paper also investigates two parameter sets, termed "original" and "modified," to analyze their impact on PEM fuel cell efficiency.

## 2. Problem statement

According to the literature, expansion and contraction of the flow channels in terms of the so-called "converging-diverging" and "tapered" flow channel configurations have shown great potential to enhance fuel cell performance. Fig.1 shows a schematic of the flow channel for conventional parallel, converging-diverging, and tapered flow configurations. Fig.1d and 1e show two novel partial converging-diverging and tapered channels named here "and "respectively. The average area of the channel is the same as before.

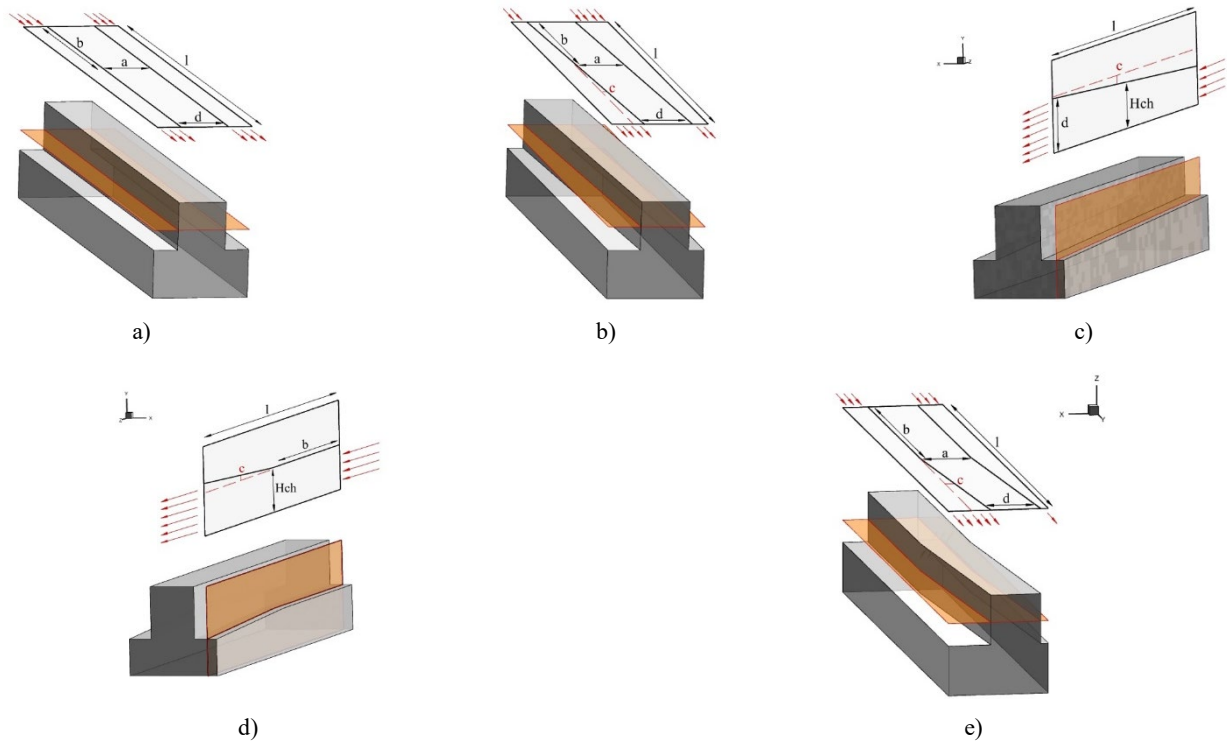


Fig.1: Variation of the pressure in the x-z plane in the middle of the cathode gas diffusion layer for a) Conventional b) Converging/diverging c) Tapered d) Half-tapered e) Half converging-diverging

## 3. Governing equations

Modeling the physical phenomena in the PEMFC requires a detailed description of a multi-component, two-phase flow model, the electrochemical reactions, the phase change rates between different states of water, the charge transfer rate, and the current density. In a multi-phase fluid flow model, each phase follows the conservation of mass and momentum. The governing equations of the present model are as follows [8]–[10]:

Mass conservation equation of gas mixture:

$$\frac{\partial}{\partial t} (\varepsilon(1-s)\rho_g) + \nabla \cdot (\rho_g \vec{u}_g) = S_m \quad (1)$$

Momentum conservation equation of gas mixture:

$$\frac{\partial}{\partial t} \left( \frac{\rho_g \vec{u}_g}{\varepsilon(1-s)} \right) + \nabla \cdot \left( \frac{\rho_g \vec{u}_g \vec{u}_g}{\varepsilon^2(1-s)^2} \right) = -\nabla p_g + \nabla \bar{\tau} + S_u \quad (2)$$

**Species conservation equation of gas mixture:**

$$\frac{\partial \left( (1-s) \rho_g Y_k \right)}{\partial t} + \nabla \cdot (\rho_g \vec{u}_g Y_k) = \nabla \cdot (\rho_g D_k^{eff} \nabla Y_k) + S_k \quad (3)$$

$$k = \text{H}_2, \text{O}_2, \text{H}_2\text{O}, \text{N}_2$$

Water dissolved transfer equation in the membrane:

$$\frac{\partial}{\partial t} \left( \varepsilon_i M_{w, \text{H}_2\text{O}} \frac{\rho_i}{EW} \lambda \right) + \nabla \cdot \left( \tilde{\tau}_m \frac{n_d}{F} M_w \right) = \nabla \cdot (M_w D_w^i \nabla \lambda) + S_\lambda + S_{gd} + S_{ld} \quad (4)$$

Mass conservation equation of liquid water:

$$\frac{\partial}{\partial t} (\varepsilon \rho_l s) + \nabla \cdot (\rho_l D_s \nabla s) + \nabla \cdot (f(s) \rho_l \vec{u}_g) = S_{gl} - S_{ld} \quad (5)$$

Conservation of electronic and protonic charge:

$$\begin{cases} \nabla \cdot (-\sigma_s^{eff} \nabla \varphi_s) = R \\ \nabla \cdot (-\sigma_m^{eff} \nabla \varphi_m) = -R \end{cases} \quad (6)$$

In the above equations,  $\rho_g$ ,  $\vec{u}_g$ ,  $p_g$  and  $\bar{\tau}$  are gas mixture density, velocity vector, pressure and viscous stress tensor respectively. The parameters  $\varepsilon$ ,  $s$ ,  $Y_k$  and  $D_k^{eff}$  represent the porosity, liquid saturation, mass fraction and effective diffusion coefficient. In addition,  $\lambda$ ,  $n_d$ ,  $D_w^i$ ,  $S_\lambda$  is the membrane water content, electrostatic drag coefficient, water diffusion coefficient, water production source term due to the reaction occurring in the cathode catalyst layer. The source term  $S_u$ ,  $S_m$ ,  $S_k$  represent the Darcy's drag force, changes in gas phase mass due to consumption/production in the electrochemical reaction and phase change respectively. The mass transfer between water vapor, liquid water, and water dissolved in ionomer are also expressed by  $S_{gl}$ ,  $S_{gd}$  and  $S_{ld}$ . In Equation (5),  $f(s)$  is the interphase drag coefficient and  $D_s$  represents the capillary diffusion coefficient. The volumetric current density  $R$  appears as the source terms in Equation (6).  $\sigma_s^{eff}$  and  $\sigma_m^{eff}$  are the effective electrical conductivity of the solid material and polymer membrane. Also,  $\varphi_s$  and  $\varphi_m$  are the electrical potential in the solid and membrane phase, respectively.

## 4. Results and Discussions

In this paper, building different flow channel types, we compare the performance pressure, variation of the mass fraction of  $\text{O}_2$ , variation of the liquid saturation, and variation of the current flux density magnitude. Fig.3 shows the pressure change along the x-z plane at the cathode gas diffusion layer in different layouts but always using the same amount of current. Fig.3a represents a conventional fuel cell where the pressure contour is symmetric around the z-axis, meaning that the pressure distribution for the neighboring channels is the same. In Fig.3b, the pressure at the converging channel is higher than that in the diverging adjacent channel. This last layout is characterized by a central wall rotated by an angle of  $0.2^\circ$  compared to the conventional fuel cell. In Fig.3g, the layout is changed; from the inlet to half of the plane, the layout is the same as the one in the conventional fuel cell, and from the half to the outlet, the layout is the same as the one of the converging/diverging. This configuration significantly increases the pressure at the inlet and consequently increases the average pressure, bringing it to the highest value (104,6 pa) if compared to the other layout. The result changes when we change the gas influx, putting it from the outlet as in Fig. 3h. This layout decreases the maximum pressure of the fuel cell at the same plane. Fig.3c shows the pressure distribution in the expanding tapered layout, seeing that the trend is like the conventional layout. Changing the influx direction from the output makes it evident how the pressure is always higher near the inlet gas part of the fuel cell. Fig.3e and 3f show the pressure changing in the half-tapered layout using an inlet from the bottom and the top. Analyzing the average pressure reported in Tab. 5 showed that the numbers are very similar for all the tapered and half-tapered layouts,

swaying between 70-71 pa. For the converging-diverging and half-converging-diverging layouts, the average pressure increases slightly, touching 90-100 pa. Thus, we can conclude that the pressure drop is not huge and will not lead to power consumption.

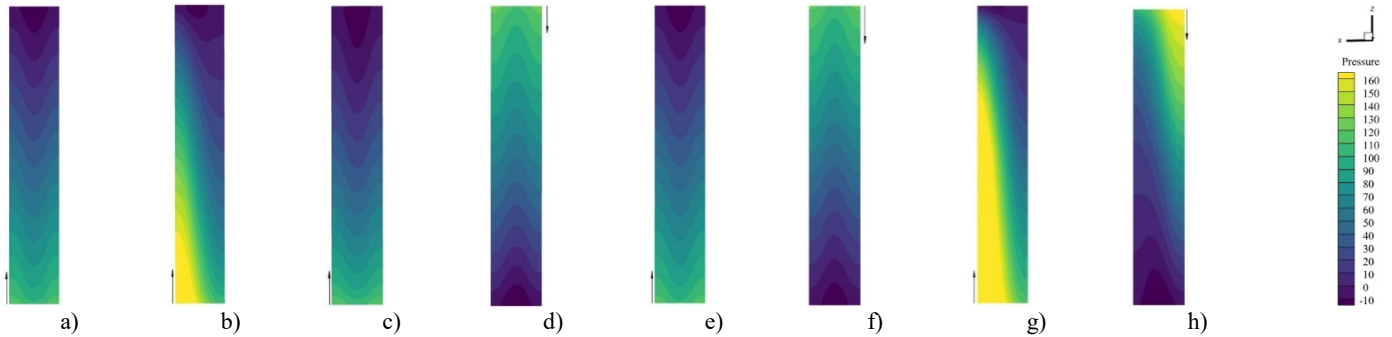


Fig.3: Variation of the pressure in the x-z plane in the middle of the cathode gas diffusion layer for a) Conventional b) Converging/diverging c) Tapered d) Tapered reverse flow direction e) Half-tapered f) Half-tapered reverse direction g) Half converging-diverging and h) Half converging-diverging reverse direction(const)

Fig.4 shows the pressure change along the mass fraction of o2 in the x-z plane in the middle of the cathode gas diffusion layer. Fig.4a has the worst uniform o2 distribution along this referential plane; there is an evident higher concentration of o2 at the inlet. We calculated and compared the average of O2 in the gas diffusion layer in all the layouts and figured out that the minimum valor is in the conventional layout for gas diffusion and catalyst layers, with 0.4 for the catalyst layer and 0.6 for the gas diffusion layer. At the same time, the maximum is touched by the converging-diverging layout with 0.15 for both the gas diffusion layer and the catalyst layer. In Fig.4b, the image shows the best distribution of the o2 and testing half of the converging-diverging layout with half conventional layout as in Fig.4g and 4h; the concentration starts to be less uniform distributed. This effect of the decreased uniform distribution of the o2 along the referential plan in the half configurations compared to the full one could also be seen in the tapered layout presented in Fig.4c, d, e, and f.

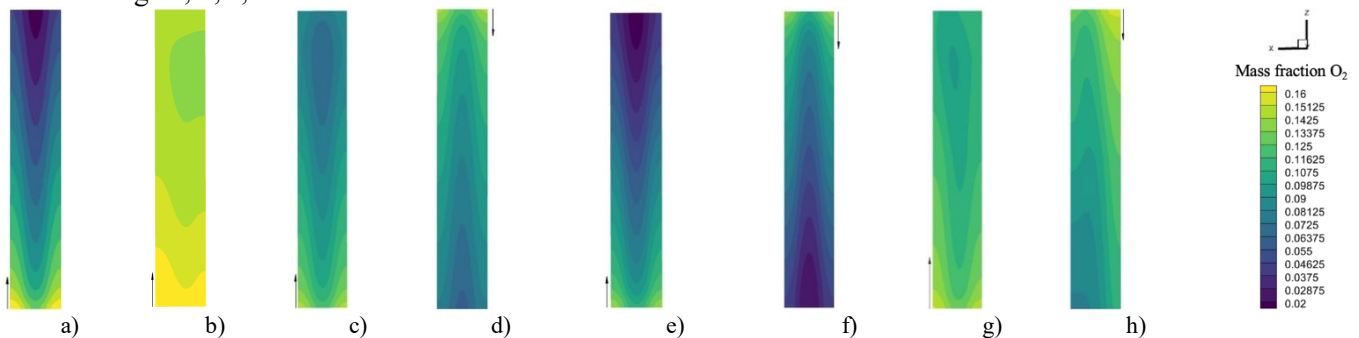


Fig.4: Variation of the mass fraction of o2 in the x-z plane in the middle of the cathode gas diffusion layer for a) Conventional b) Converging/diverging c) Tapered d) Tapered reverse flow direction e) Half-tapered f) Half-tapered reverse direction g) Half converging-diverging and h) Half converging-diverging reverse direction(const)

Fig.5 shows the variation of the liquid saturation in the x-z plane in the middle of the cathode gas diffusion layer. The best performance can be seen in Fig.5f and 5e, in which we have an average lower liquid saturation. In all cases, the liquid saturation has a higher valor that is distributed and follows the wall part of the flow cathode layer. The worst performance can be seen in Fig.5g, 5d, and 5h. Net of all that, we have also calculated the average saturation in the gas

diffusion layer and catalyst layer, noticing that they are almost the same; they are respectively in a range of 0.10 in the first layer and 0.14/0.15 in the second.

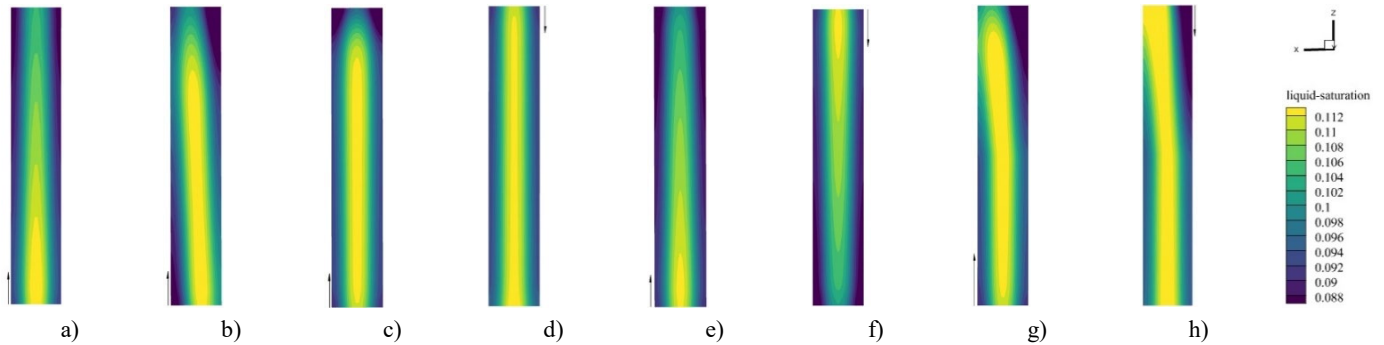


Fig.4: Variation of the liquid saturation in the x-z plane in the middle of the cathode gas diffusion layer for a) Conventional b) Converging/diverging c) Tapered d) Tapered reverse flow direction e) Half-tapered f) Half-tapered reverse direction g) Half converging-diverging and h) Half converging-diverging reverse direction(const)

Fig.6 illustrates the potential distribution of hydrogen/air fuel cells over the cell cross-section. Fig.7a compares the conventional, converging/diverging, and tapered layouts. We can see that at higher currents (higher than 1.5 A/cm<sup>2</sup>), the conventional layout has the worst performance, and the converging-diverging one correlates with higher voltage. With lower current values, the trend in the three layouts is the same; the conventional layout starts to underperform, compared to the other two cases, from a current of 1 A/cm<sup>2</sup>). In Fig.7b, there is a comparison between four different tapered layouts. The half versions of this layout are less efficient at currents higher than 1.5 A/cm<sup>2</sup>. With less current, the trends of the three layouts are very similar. Still, from a current of 1.7, voltage values of the tapered layout with an inflow that has an opposite direction compared to the tapered, whose trend is green, are higher than all the other configurations. Fig.6c compares the convergent/diverging, half-convergent/diverging, and half-convergent-diverging reverse-direction layouts. From a current of 1.1A/cm<sup>2</sup> and going up, the convergent/Diverging layouts perform best. The directions of the influx in the half layout in Fig.7c do not influence the trend, making it remain the same.

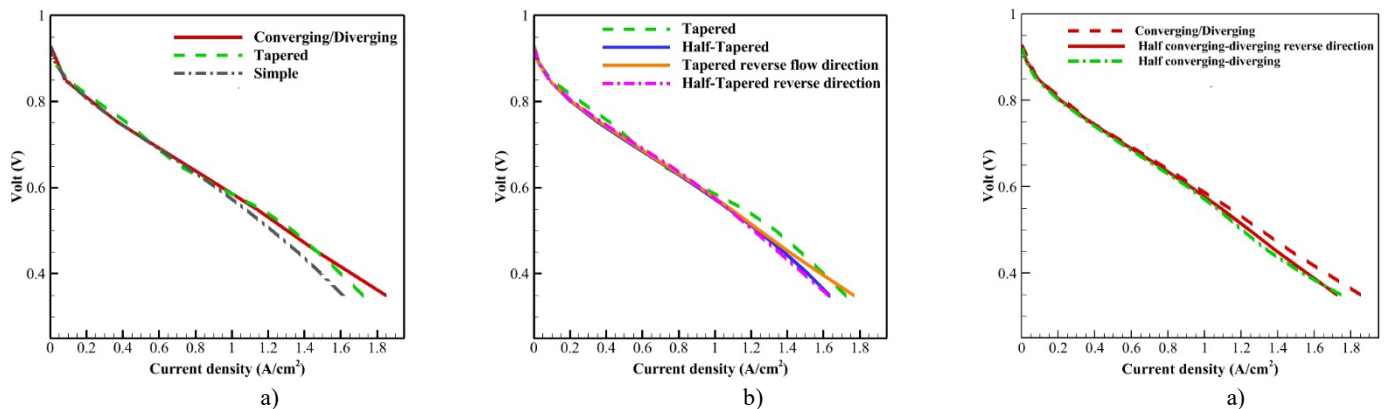


Fig.7: Comparison of voltage-current curve for a) Conventional, Converging/Diverging, Tapered b) Tapered, Tapered reverse flow direction, Half-Tapered, Half-Tapered reverse direction and c) Converging/Diverging, Half converging/diverging, Half converging-diverging reverse direction.

## 5. Conclusion

In this paper, a comparison is made between the performance of a conventional parallel flow field and various flow fields with contraction/expansion in the channel. Based on the numerical simulation results, an analysis of the V-I curve,

pressure, and O<sub>2</sub> concentration contours, and liquid water saturation distribution in the catalyst layer was performed. It is concluded that all types of contracted/expanded flow fields produce higher maximum power than the parallel flow field. The positive effect occurs at high current densities when concentration losses predominate.

## Acknowledgments

Bagherighajari acknowledges Ph.D. scholarship with the reference number 2022.09877.BD from FCT-Foundation for Science and Technology, Authors acknowledge the support received within the FCT advanced computing project with the Ref. 2023.10385.CPCA.A0 and authors also acknowledge the financial support from by C-MAST (Center for Mechanical and Aerospace Science and Technology), Research Unit No. 151, Project Grant No. UIDB/00151/2020 (<https://doi.org/10.54499/UIDB/00151/2020>) and Grant No. UIDP/00151/2020 (<https://doi.org/10.54499/UIDP/00151/2020>), Funding 2025-2029, transition period.

## References

- [1] “Global Energy Review: CO<sub>2</sub> Emissions in 2021 – Analysis - IEA.” [Online]. Available: <https://www.iea.org/reports/global-energy-review-co2-emissions-in-2021-2>. [Accessed: 01-Dec-2024].
- [2] L. Zhang and Z. Shi, “Optimization of serpentine flow field in proton-exchange membrane fuel cell under the effects of external factors,” *Alexandria Eng. J.*, vol. 60, no. 1, pp. 421–433, Feb. 2021.
- [3] S. Abdulla and V. S. Patnaikuni, “Performance evaluation of Enhanced Cross flow Split Serpentine Flow Field design for higher active area PEM fuel cells,” *Int. J. Hydrogen Energy*, vol. 45, no. 48, pp. 25970–25984, Sep. 2020.
- [4] K. S. Choi, H. M. Kim, and S. M. Moon, “Numerical studies on the geometrical characterization of serpentine flow-field for efficient PEMFC,” *Int. J. Hydrogen Energy*, vol. 36, no. 2, pp. 1613–1627, Jan. 2011.
- [5] Z. Zhang, F. Bai, P. He, Z. Li, and W. Q. Tao, “A novel cathode flow field for PEMFC and its performance analysis,” *Int. J. Hydrogen Energy*, vol. 48, no. 63, pp. 24459–24480, Jul. 2023.
- [6] Y. Xu, L. Peng, P. Yi, and X. Lai, “Analysis of the flow distribution for thin stamped bipolar plates with tapered channel shape,” *Int. J. Hydrogen Energy*, vol. 41, no. 9, pp. 5084–5095, Mar. 2016.
- [7] C. Wang, Q. Zhang, J. Lu, S. Shen, X. Yan, F. Zhu, X. Cheng, and J. Zhang, “Effect of height/width-tapered flow fields on the cell performance of polymer electrolyte membrane fuel cells,” *Int. J. Hydrogen Energy*, vol. 42, no. 36, pp. 23107–23117, Sep. 2017.
- [8] F. Bagherighajari, A. Ramiar, M. Abdollahzadehsangroudi, J. C. Páscoa, and P. J. Oliveira, “Numerical simulation of the polymer electrolyte membrane fuel cells with intermediate blocked interdigitated flow fields,” *Int. J. Energy Res.*, 2022.
- [9] A. M. Bilondi, F. Bagherighajari, M. Abdollahzadeh, M. J. Kermani, and J. C. Pascoa, “The role of porous carbon inserts on the performance of polymer electrolyte membrane fuel cells: a parametric numerical study,” *Energy Technol.*, vol. 10, p. 2200966, 2022.
- [10] F. Rodrigues, M. Abdollahzadeh, F. Bagherighajari, and J. Pascoa, “Numerical Simulation of Anti-Icing Effect With Dielectric Barrier Discharge Plasma Actuators on a Surface of an Airfoil,” in *Proceedings of the ASME 2022 Fluids Engineering Division Summer Meeting. Volume 1: Fluid Applications and Systems (FASTC); Fluid Measurement and Instrumentation (FMITC); Fluid Mechanics (FMTC).*, 2022, p. V001T03A035.